EFFECT OF MICROSTRUCTURE ON FRACTURE TOUGHNESS OF AGE-HARDENED ALLOYS

A. Gysler*, V. Bachmann**, G. Lütjering*

The influence of grain size, phase dimensions and morphology on the fracture behavior of age-hardened Ti-8.6Al, Ti-6Al-4V, and Al-5.9Zn-2.6Mg-1.7Cu alloys was investigated. Furthermore the effects of ΔK variations during pre-cracking and of environment on the fracture behavior are reported. A reduction in grain or phase dimensions increased the K_O-values to initiate crack extension from the fatigue notch, while further crack extension resistance was dependent on the grain size effect on fracture mode. The K-values were not significantly affected by ΔK-variations, but corrosive environments decreased the crack extension resistance.

INTRODUCTION

The importance of microstructural control with regard to the fracture behavior of high-strength alloys is well documented by a number of review articles concerning Al-alloys (1), Ti-alloys (2), and high strength steels (3). The important microstructural parameters are the size and distribution of inclusions, degree of age-hardening, grain size and shape, texture, phase dimensions and morphology in multiphase alloys, phase stability against stress-induced transformations, and impurity atoms leading to grain boundary embrittlement. Which of these parameters are dominating depends on the particular alloy system.

However, the grain size or phase dimensions seem to play a significant role with regard to fracture toughness in many cases. There are indications in the literature that refining the grain size results in an increase in fracture toughness of Al-alloys (4,5), as well as of steels (3,6). On the other hand the experimental results reported for Ti-alloys seem to be contradictory (2,7).

The purpose of the present work was to contribute to the understanding of the effects of microstructure on the fracture behavior of age-hardened alloys. Furthermore, since crack extension in a fracture toughness test starts from a fatigue precracked notch, it seemed necessary to clarify first the role which the cyclic stress intensity factors during pre-cracking and the environmental test conditions are playing.

*Technische Universität Hamburg-Harburg, D-2100 Hamburg 90
**DFVLR, Institut für Werkstoff-Forschung, D-5000 Köln 90

EXPERIMENTAL PROCEDURE

The tests were performed on three different alloys: Ti-8.6Al (chemical composition in wt.%), which was quenched from 900°C and aged at 500°C for 10h; Ti-6Al-4V, which was processed to obtain five different phase structures. The quenching temperature for all five conditions was 800°C followed by aging at 500°C for 24h. The third alloy, Al-5.9Zn-2.6Mg-1.7Cu, containing less than 0.01 wt.% each of Cr, Fe, and Si, was quenched from 440°C and aged at 100°C for 24h. Details of the chemical analysis, and the rolling and recrystallization procedures can be found elsewhere (8,9). The grain and phase dimensions, together with the tensile properties are summarized in Table 1.

All mechanical tests were performed at room temperature with the stress axis parallel to the rolling direction. Tensile tests were done on round specimens with gage dimensions of 4 mm diameter and 25 mm length and an initial strain rate of $8 \times 10^{-4} s^{-1}$. Fracture toughness tests were carried out on CT-specimens having a thickness B of 6 mm and a width W of 32 mm. The fatigue pre-cracking ($R = 0.2$, $f = 30$ Hz) and the fracture toughness tests were done on a closed-loop servohydraulic testing machine. The length of the fatigue pre-crack from the chevron notch was at least 3 mm resulting in a total notch length of about 0.5 W. The constant cross-head displacement velocity (1mm/min) gave a rate of stress intensity increase of 1.7 $MPa \cdot m^{1/2} s^{-1}$. The load F was monitored as a function of crack opening displacement COD, measured with a clip-gage. The reported fracture toughness values are the average of at least two tests, unless otherwise stated. For some tests the crack extension Δa was determined using the electric potential method. Most of the fracture toughness tests were carried out in vacuum ($< 10^{-4}$ Pa), with additional tests in laboratory air and 3.5% NaCl solution to determine the influence of an aggressive environment.

TABLE 1 - Grain or Phase Dimensions and Tensile Properties

Alloy (wt.%)	Grain or Phase Dimensions (μm)	$\sigma_{0.2}$ (MPa)	σ_F (MPa)	$\varepsilon_F = \ln(A_O/A_F)$
Ti-8.6Al	45	825	929	0.15
	110	757	815	0.09
Ti-6Al-4V	1 - 2	1150	1545	0.74
	10 - 12	1073	1410	0.55
	6*	1005	1455	0.61
	2**	1088	1267	0.11
	12**	902	1194	0.31
Al-5.9Zn-2.6Mg-1.7Cu	36	420	840	0.65
	220	420	720	0.35

* Primary α-grain size
** Width of lamellar α-phase

To investigate the crack tip configuration in the plane strain region, some specimens were loaded to a defined stress intensity factor K, unloaded, and sectioned in the mid-thickness (0.5 B). Samples containing the crack tip areas were mechanically polished and ion beam milled. Scanning electron microscopy (SEM) studies were performed on ion beam milled and on additionally slightly etched pieces to investigate the crack tip configuration in early stages of crack extension under monotonic loading.

RESULTS AND DISCUSSION

Effect of Test Conditions on Fracture Behavior

In order to understand the effects of crack tip geometry and material condition ahead of the crack tip after fatigue pre-cracking on the resulting fracture behavior the cyclic stress intensity factor ΔK was varied. Since it is known from fatigue crack propagation tests that the environmental condition can drastically affect the fracture behavior at the crack tip (10), tests were carried out in inert (vacuum) as well as in corrosive environments (air, NaCl solution). These tests were done on Ti-8.6Al with a small grain size of 45 µm and on Ti-6Al-4V with a fine equiaxed grain structure of 1 - 2 µm (Table 1).

The results for the Ti-Al alloy are summarized in Table 2, which shows ΔK; $K_f(max)$, the maximum stress intensity factor during cycling; K_o and K_5, the stress intensity factors at the beginning of crack extension; K_m, the maximum stress intensity factor where unstable fracture occurred, and the environment during pre-cracking and fracture toughness test.

From Table 2 it can be seen that a variation of ΔK from 15 to 44 MPa·m$^{1/2}$ in vacuum and from 9 to 19 MPa·m$^{1/2}$ in NaCl solution resulted only in a slight increase of the K-values. For example in vacuum K_o increased from 48 to 52 MPa·m$^{1/2}$, and in NaCl from 16 to 19 MPa·m$^{1/2}$. Such small effects of ΔK on the fracture behavior of the Ti-Al alloy indicate that the crack tip configurations and the material conditions ahead of the tip due to fatigue pre-cracking are not affecting the fracture behavior in a significant way.

The effect of environment on the fracture behavior of Ti-Al was found to be very pronounced, as can be seen from the results in Table 2. For example the K_o-value dropped from 48 MPa·m$^{1/2}$ in vacuum to 16 MPa·m$^{1/2}$ in NaCl solution. The K_5- and K_m-values also

TABLE 2 - Effect of Fatigue Pre-Cracking and Environment on Fracture Toughness of Ti-8.6Al (10h 500°C, G.S. 45µm)

ΔK (MPa·m$^{1/2}$)	$K_f(max)$ (MPa·m$^{1/2}$)	K_o (MPa·m$^{1/2}$)	K_5 (MPa·m$^{1/2}$)	K_m (MPa·m$^{1/2}$)	Environment
15	19	48	57	61	Vacuum
44	55	52	62	64	Vacuum
9	11	16	22	30	NaCl
19	24	19	23	26	NaCl

showed similar differences between tests in vacuum and salt solution (Table 2). SEM studies of specimens tested in salt solution revealed that the entire fracture surface created during monotonic loading exhibited a step-like fracture mode typical for fracture of Ti-Al alloys in NaCl solution. Since the plastic zone size resulting from fatigue pre-cracking is much smaller than the observed crack extension during monotonic loading the environmental influence was also dominant during the fracture toughness test. Therefore the K_m-values were lower in salt solution than in vacuum (Table 2).

The reason for the significant decrease in resistance against crack extension in NaCl solution is thought to be due to an hydrogen embrittlement process resulting from hydrogen atoms swept into the plastic zone by moving dislocations (11).

The effects of fatigue pre-cracking and environment on the fracture behavior of fine equiaxed Ti-6Al-4V are shown in Table 3. In vacuum a variation of ΔK between 8 and 23 MPa·m$^{1/2}$ did not have a significant influence on the fracture values. In laboratory air a similar ΔK-variation also showed no major effect on K_o, however, the K_m-values were significantly higher for fatigue pre-cracking at high ΔK (K_m = 77 MPa·m1/2) compared with those after pre-cracking at low ΔK (K_m = 55 MPa·m$^{1/2}$). The reason for this difference in resistance against crack propagation under monotonic loading seems to be a consequence of crack branching occurring after pre-cracking at high but not at low ΔK. This explanation was supported by SEM-studies showing extensive secondary cracking on the fatigue fracture surfaces after cycling at high ΔK but not at low ΔK. These secondary cracks are thought to induce crack branching which is known to reduce the overall crack propagation rate.

A variation of the environmental conditions for Ti-6Al-4V showed a continuous decrease of the fracture toughness values K_o and K_5 with increasing aggressiveness of the surrounding environment for fatigue pre-cracking at low ΔK (Table 3). This behavior also can be explained with an hydrogen embrittlement process at the crack tip. The K_m-values from tests in vacuum and NaCl solution exhibited only slight differences (Table 3). This can be explained with a transition in fracture mode occurring during

TABLE 3 - Effect of Fatigue Pre-Cracking and Environment on Fracture Toughness of Ti-6Al-4V (24h 500°C, Fine Equiaxed)

ΔK (MPa·m$^{1/2}$)	K_f(max) (MPa·m$^{1/2}$)	K_o (MPa·m$^{1/2}$)	K_5 (MPa·m$^{1/2}$)	K_m (MPa·m$^{1/2}$)	Environment
8.5	11	60	63	63	Vacuum
23	29	59	63	63	Vacuum
8.3	10	52	55	55	Air
23	29	54	77	77	Air
8.5	11	36	46	60	NaCl
23	29	51	56	56	Vacuum/Air
22	28	64	65	65	Air/Vacuum

stable crack extension in NaCl solution. The SEM micrograph in Fig. 1a shows the step-like fracture mode at the beginning of crack extension and the dimple type of failure mode at a later stage of crack propagation under monotonic loading (Fig. 1b). Since dimple rupture is typical for fracture of fine equiaxed Ti-6Al-4V in inert environments, it can be concluded that crack extension eventually becomes faster than the hydrogen embrittlement process. Therefore the K_m-values from tests in NaCl solution approach the K_m-values observed in vacuum (Table 3).

The influence of a corrosive environment during pre-cracking at high ΔK resulted in a slight decrease of K_o but in a significant increase of K_5 comparing the results obtained in vacuum and air (Table 3). In order to support the explanation that the increase of K_m from 63 MPa·$m^{1/2}$ in vacuum to 77 MPa·$m^{1/2}$ in air resulted from crack branching during monotonic loading as a consequence of secondary cracks observed on the fatigue fracture surface after pre-cracking in air, additional tests were carried out. Fatigue pre-cracking at high ΔK was performed in vacuum while the fracture toughness test was done in air and vice versa. As shown in Table 3 the K_m-value was again higher for pre-cracking in air compared with that after pre-cracking in vacuum. This indicates that the environmental influence during pre-cracking at high ΔK determines the concomitant fracture toughness value and not the environment during monotonic loading. It should be noted, however, that only one specimen was used for these tests and the results can therefore be considered as preliminary ones only.

Effect of Microstructure on Fracture Toughness

The test conditions for studying the correlation between microstructure and fracture behavior were kept constant; fatigue pre-cracking was done at low ΔK, resulting in fatigue crack propagation rates of about 2 x 10^{-6} mm/cycle, and all tests reported here were performed in vacuum.

Effect of grain size. Average fracture toughness values for the age-hardened Ti-Al alloy with grain sizes of 45 and 110 µm are summarized in Table 4. The results indicate that the energy to extend the crack from the fatigue pre-crack was higher for the fine grain size material (K_o = 48 MPa·$m^{1/2}$) compared with the coarse grain structure (K_o = 41 MPa·$m^{1/2}$). However, further crack extension under monotonic loading was easier in the fine grain size material resulting in K_5- and K_m-values of 58 and 60 MPa·$m^{1/2}$ respectively, while the corresponding values for the coarse structure were 71 and 82 MPa·$m^{1/2}$.

Crack propagation under monotonic loading in the plane strain region of Ti-Al occurred mainly along grain boundaries independent of grain size. The crack tip configuration in the plane strain region of specimens loaded to K_5 are shown in Figs. 2a and b for fine and coarse grain size materials. Although these micrographs were taken from specimens without applied load it seems that crack extension occurs by a crack nucleation process along grain boundaries ahead of the crack tip. Assuming such a model then the higher K_o-values observed for a fine grain structure are a consequence of the higher applied stresses necessary to reach the local fracture stress at the head of dislocation pile-ups against grain

TABLE 4 - Effect of Grain Size on Fracture Behavior of Ti-8.6Al (10h 500°C)

Grain Size (μm)	K_o (MPa·m1/2)	K_5 (MPa·m1/2)	K_m (MPa·m1/2)
45	48	58	60
110	41	71	82

boundaries due to the smaller pile-up lengths. Further crack extension could then be easier in a material with a small grain size, since the density of microcracks ahead of the crack tip must be higher due to the higher number of grain boundaries per volume in a fine grain size material. It should be noted that the higher percentage of shear fracture mode observed for the coarser microstructure can also contribute to the higher K_5- and K_m-values in comparison to those for the small grain size material (Table 4).

The effect of grain size on the fracture behavior of the age-hardened Al-Zn-Mg-Cu alloy is demonstrated in Fig. 3 as plots of K versus Δa. The resistance against crack extension was higher for the material with a small grain size. However the K_m-values, where unstable fracture was observed, were approximately the same (about 78 MPa·$m^{1/2}$).

Fracture surface investigations revealed that the fracture modes within the plane strain regions were different for both grain size structures. Specimens with a small grain size fractured predominantly by dimple rupture (Fig. 4a), while the material with a coarse structure exhibited a fracture topography showing portions of grain boundary fracture as well as dimple rupture (Fig. 4b). The higher resistance against crack extension of the small grain size material seems to result from the higher energy necessary for void nucleation and growth ahead of the crack tip, while the portions of low energy absorbing intergranular failure in the coarse structure lowered the crack extension resistance.

The similar K_m-values observed in Fig. 3 seem to be due to a transition from fracture under plane strain to fracture under plane stress in the later stages of crack extension in both materials. Fracture surface studies showed that in the regions where the shear mode failure was dominating a complete dimple type of fracture mode occurred, independent of grain size.

Effect of phase morphology and dimensions. The resistance against fracture as a function of crack extension for the five different microstructures of the (α+β) alloy, Ti-6Al-4V, are shown in Fig. 5. The highest K_o-value was found for the fine equiaxed structure (58 MPa·$m^{1/2}$), while the coarse equiaxed, and bi-modal microstructures exhibited lower values of 50 and 48 MPa·$m^{1/2}$, respectively. The lamellar structures showed even lower K_o-values of 46 MPa·$m^{1/2}$ for coarse and 38 MPa·m1/2 for fine phase dimensions (Fig. 5).

The resistance against further crack extension under monotonic loading was about similar for coarse equiaxed and bi-modal

structures, as can be seen from the almost identical slopes of the K versus Δa curves in Fig. 5. However the K_m-value was higher for the bi-modal structure (125 MPa·$m^{1/2}$) compared with 104 MPa·$m^{1/2}$ for the coarse equiaxed microstructure. The fine equiaxed phase structure revealed a much lower resistance against crack extension and fractured in an unstable way at about 62 MPa·$m^{1/2}$. On the other hand the coarse lamellar microstructure exhibited a very pronounced crack extension of about 3 mm before failing in an unstable manner at 130 MPa·$m^{1/2}$. The fine lamellar structure fractured already at a K_m-value of only 58 MPa·$m^{1/2}$ (Fig. 5).

The results from Fig. 5 will be discussed for the equiaxed and bi-modal microstructures first. The variation of K_o can be explained through the differences in α-phase dimensions between the three microstructures. Assuming that crack nucleation under monotonic loading occurred at slip band/grain boundary intersections, then the resistance against crack extension from the fatigue pre-crack should be higher for smaller grain size materials, similar as discussed for Ti-Al. This is confirmed through the experimental observations which showed higher K_o-values for fine equiaxed compared with those of the coarser structures in Fig. 5.

Crack extension in all three equiaxed microstructures takes place through microvoid nucleation and growth. The significantly lower resistance against crack extension of the fine equiaxed structure (Fig. 5) can then be explained qualitatively. Compared with a coarser structure the fine equiaxed microstructure contains a larger number of prospective void nucleation sites per volume and therefore a higher volume fraction of holes ahead of the crack tip. It seems reasonable that less energy will be consumed to connect these closely spaced pores compared with a coarser structure where the volume fraction of holes is much lower. The high K_m-value of the bi-modal structure seems to result from the existence of the lamellar regions between the primary α-grains which delay the growth process of voids. The higher percentage of shear fracture mode also can contribute to the observed higher crack extension resistance of the coarser Ti-6Al-4V microstructure in Fig. 5 similar as mentioned for the Ti-Al alloy.

The results of the lamellar microstructures in Fig. 5 will be discussed only very briefly, since more investigations seem to be necessary to explain the significantly lower resistance against crack extension of the fine compared with the coarse lamellar structure. The crack tip configurations in the plane strain regions after loading to a stress intensity factor K_5 are almost identical for both microstructures as can be seen from the micrographs in Fig. 6. Therefore a higher amount of crack branching of the coarse lamellar microstructure to account for the higher crack extension resistance cannot be considered as a reasonable explanation. The only parameter variation which seems to predict the ranking of the two curves in Fig. 5 is the large, and unexpected difference in tensile ductility between fine (ε_F = 0.11) and coarse (ε_F = 0.31) lamellar microstructures (Table 1).

CONCLUSIONS

1. Fatigue pre-cracking at low or high cyclic stress intensity factors did not significantly affect the fracture toughness

values as long as no secondary cracking during cycling was observed. However, if secondary cracks occurred during fatigue pre-cracking the fracture toughness values were significantly higher due to crack branching.

2. Aggressive environments (air, salt solution) reduced the resistance against crack extension compared with the results obtained in vacuum. In order to obtain valid design data it is suggested therefore to perform fracture toughness tests in the same environment as the material will be applied.

3. A grain refinement increased the K_O-values of equiaxed Ti-alloys, and of Al-alloys. The resistance against further crack extension was lower for small grain size materials if the fracture mode was not changed through the grain refinement.

ACKNOWLEDGMENT

This work was supported by the Electric Power Research Institute, Palo Alto, CA., U.S.A., under contract RP 1266-1.

REFERENCES

1. Hahn,G.T., and Rosenfield,A.R.,1975,Met.Trans.6A,653.

2. Stubbington,C.A.,1975,"Metallurgical Aspects of Fatigue and Fracture of Titanium Alloys",AGARD Conference Proceedings No.185.

3. Zackay,V.F.,1975,"Fundamental Considerations in the Design of Ferrous Alloys",AGARD Conference Proceedings No.185.

4. Kaufman,J.G.,1975,"Design of Aluminum Alloys for High Toughness and High Fatigue Strength",AGARD Conference Proceedings No.185.

5. Kawabata,T., and Izumi,O.,1978,J.Mat.Sci.13,945.

6. Webster,D.,1969,Trans.ASM 62,759.

7. Greenfield,M.A., and Margolin,H.,1971,Met.Trans.2,841.

8. Gysler,A., and Lütjering,G.,1982,Met.Trans.13A,(in press).

9. Lütjering,G.,Hamajima,T., and Gysler,A.,1977,"Influence of Grain Size on the Fracture of Aluminum Alloys",Fracture 1977, Vol.2,7.

10. Lindigkeit,J.,Terlinde,G.,Gysler,A., and Lütjering,G.,1979, Acta Met.27,1717.

11. Tien,J.K.,Thompson,A.W.,Bernstein,I.M., and Richards,R.J., 1976,Met.Trans.7A,821.

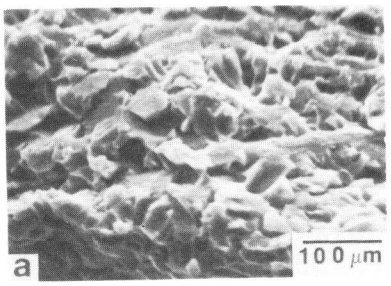

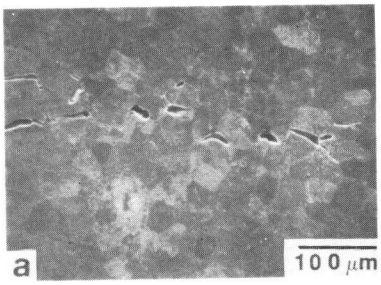

——— Crack Propagation Direction ⟶

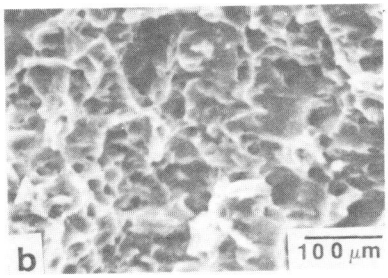

Fig.1 Ti-6Al-4V, 24h 500°C,NaCl; a)Δa < 0.5mm b)Δa > 1mm (SEM)

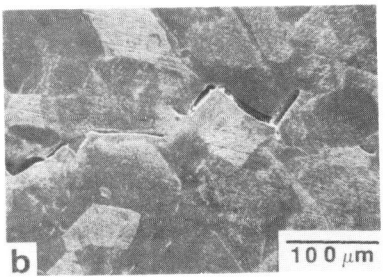

Fig.2 Ti-8.6Al, 10h 500°C,Vacuum; a)G.S. 45μm b)G.S. 110μm (SEM)

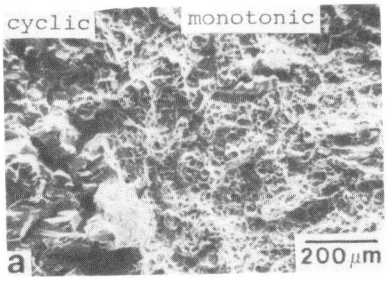

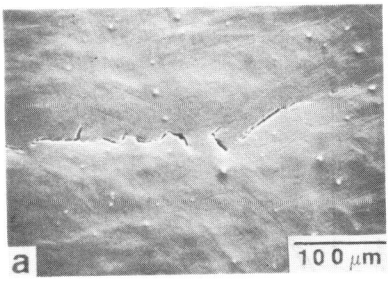

——— Crack Propagation Direction ⟶

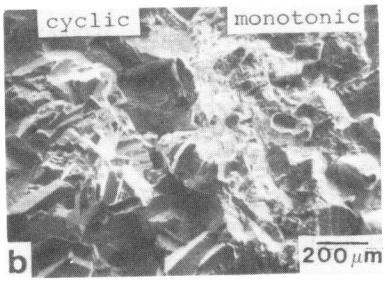

Fig.4 Al-Zn-Mg-Cu, 24h 100°C, Vacuum; a)G.S. 36μm b)G.S. 220μm

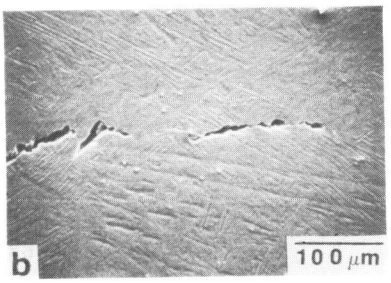

Fig.6 Ti-6Al-4V, 24h 500°C,Vacuum; a)fine lamellar b)coarse lamellar

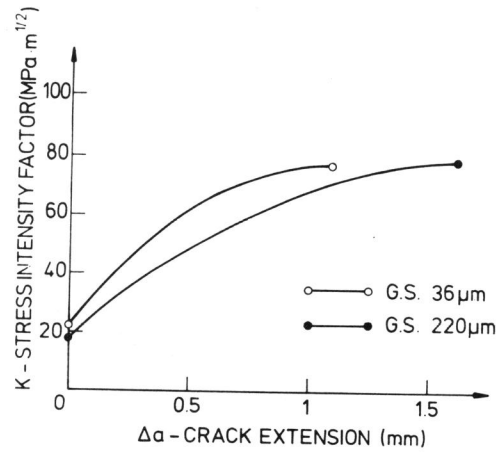

Fig.3 Al-Zn-Mg-Cu, 24h 100°C, Vacuum

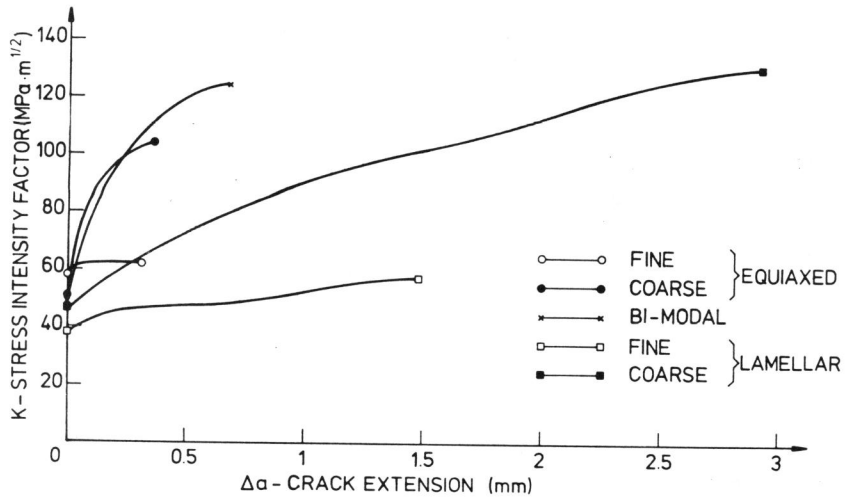

Fig.5 Ti-6Al-4V, 24h 500°C, Vacuum